AN INVESTIGATION OF ALGEBRAIC TURBULENCE AND TURBULENT SCALAR-FLUX MODELS FOR COMPLEX FLOW FIELDS WITH IMPINGEMENT AND SEPARATION

Ken-ichi Abe
Department of Aeronautics and Astronautics,
Kyushu University
Hakozaki, Higashi-ku, Fukuoka 812-8581, Japan
abe@aero.kyushu-u.ac.jp

ABSTRACT

Algebraic relations that link the scalar-flux components to mean scalar gradient were investigated in several complex turbulent flows with impingement and separation. To illustrate the characteristics of the models, three flow configurations were selected, i.e., a fully-developed plane channel flow, a plane impinging jet and a separated flow around an obstacle in a plane channel, for all of which LES data were available for comparison as wall as for a priori test.

Previous studies have pointed out that higher turbulent Prandtl number or similar effect needs to be incorporated into the models for reasonable scalar-transfer predictions in the regions around stagnation and reattachment points. Such treatments commonly have the capability of reducing an excessive turbulent length scale for the scalar-field prediction.

The present investigations, however, indicate that model constants at the same level as in the channel-flow case may be used for predicting scalar fluxes even in complex turbulence with impingement and separation.

INTRODUCTION

Reynolds-averaged turbulence models continue to constitute the principal approach for representing the effects of turbulence in prediction procedures for engineering flows. One issue that has been the subject of much attention is the wall-limiting behavior returned by low-Reynolds-number forms that are designed to be applicable across the viscous sublayer, down to the wall. This is of particular concern in relation to scalar transfer at walls, where the turbulence property of the near-wall layer plays a critical role.

On the other hand, recently, algebraic turbulent scalar-flux models have also developed for application to complex turbulent scalar-transfer fields. Among them, Abe and Suga (2001a, 2001b) reported some important knowledge for constructing a high-performance algebraic scalar-flux model by investigating LES data under several strain conditions, leading to a proposal of a new model expression (Suga and Abe, 2000). Although this (SA) model gave successful predictions for both components of scalar fluxes (i.e., $\overline{ut}$ and $\overline{vt}$) in several fundamental test cases including shear-free surfaces, further detailed discussion is still needed especially on its application to more complex flow fields.

The present paper is a contribution to the ongoing search for better algebraic turbulence and turbulent scalar-flux models for complex flow fields. In this study, we revisited and reevaluated some basic tensorial formulations for representing scalar fluxes algebraically. Investigations were performed by both a priori tests using LES data and actual calculations with a recently-developed algebraic velocity-field model. The characteristics of the model expressions are illustrated by application of the models to several test cases with impingement and separation.

TURBULENT SCALAR-FLUX MODELS

The generalized gradient-diffusion hypothesis (GGDH) model is expressed as follows (Daly and Harlow, 1970):

$$\overline{u_i t} = -C_{t1}\tau_t \, \overline{u_i u_j} \, \overline{T}_{,j} \tag{1}$$

where $\overline{T}$, $\overline{u_i t}$ and $\overline{u_i u_j}$ are the mean scalar, the turbulent scalar-flux vector and the Reynolds-stress tensor, respectively. In Eq. (1), C_{t1} and τ_t are a model coefficient and a characteristic time scale, respectively. Although the GGDH model has been most often adopted in many engineering applications, one crucial problem is that it gives an extreme underprediction of the streamwise scalar flux ($\overline{ut}$) even in simple wall-shear flows (see for example, Launder, 1976).

Considering the fact that the scalar fluctuation (t) in the wall-shear region correlates more strongly with the streamwise velocity fluctuation (u) than with the wall-normal one (v) (Kim and Moin, 1989), Abe and Suga (2001a) suggested that the introduction of the following expression into a model was effective to improve the predictive performance:

$$\overline{u_i t} = -C_{t2}\tau_t \left(\frac{\overline{u_i u_k} \; \overline{u_k u_j}}{k} \right) \overline{T}_{,j} \tag{2}$$

where $k = (\overline{u_i u_i}/2)$ is the turbulence energy. This is regarded as a higher-order extension of the GGDH model by using the quadratic products of the Reynolds-stress tensor (quadratic model).

Taking account of these discussions, Abe and Suga (2001a) proposed a combined expression of the GGDH and the quadratic forms as

$$\overline{u_i t} = -k\tau_t \left(C_{t1} \frac{\overline{u_i u_j}}{k} + C_{t2} \frac{\overline{u_i u_k} \; \overline{u_k u_j}}{k^2} \right) \overline{T}_{,j} \tag{3}$$

and then the SA model was calibrated (Suga and Abe, 2000). After that, Abe and Suga (2001b) confirmed that the discussion on the scalar-flux vector angle was basically applicable to flow fields with impingement and separation. However, the models by Eqs. (1) (GGDH) and (2) (quadratic) have not been compared yet in such complex flows and thus detailed discussion is still needed. Hence, to reveal their characteristics in more detail, we investigated the above two expressions by applying them independently to some test cases including flow impingement and separation.

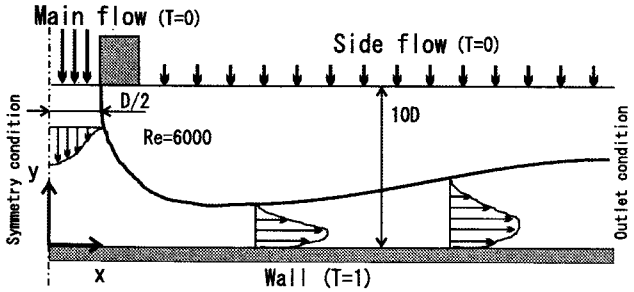

Figure 1: Plane impinging jet ($Re = U_0 D/\nu = 6000$).

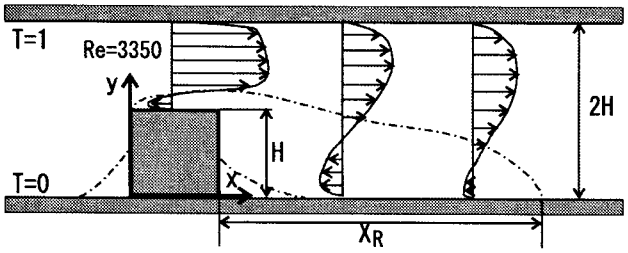

Figure 2: Obstacle flow ($Re = U_H H/\nu = 3350$).

As is seen in the SA model, most low-Reynolds-number scalar-flux models include highly-functionalized model coefficients to reproduce complex scalar-transfer phenomena very close to the wall surface. However, such model coefficients are likely to make discussion point ambiguous at the stage of fundamental investigation. Thus a simple expression for the time scale τ_t with a constant coefficient was adopted in this study.

As for C_{t1} and C_{t2}, we set constant values as $C_{t1} = 0.22$ and $C_{t2} = 0.45$, respectively. They were commonly used for all the test cases to follow. Concerning the time scale, the following expression was adopted as the first attempt (Durbin, 1993):

$$\tau_t = \max(\frac{k}{\varepsilon}, 6\sqrt{\frac{\nu}{\varepsilon}}) \tag{4}$$

where ε is the dissipation rate of k. Note that to reproduce strictly correct near-wall limiting behavior of scalar fluxes, both $C_{t1}\tau_t$ and $C_{t2}\tau_t$ need to be proportional to y^{-1} when the wall approaches. In this sense, the time scale by Eq. (4) doesn't always ensure the correct near-wall behavior, although the present results are enough to discuss on fundamental characteristics of the models.

TEST CASES AND COMPUTATIONAL CONDITIONS

To illustrate the characteristics of the models, three test cases were selected, i.e., a fully-developed plane channel flow, a plane impinging jet and a separated flow around an obstacle in a plane channel (obstacle flow), for all of which LES data (Abe and Suga, 2001a, 2001b) were available for a priori tests and also for comparison with the results presently obtained. As for the channel-flow case, the Reynolds number based on the channel width ($2H$) and the mean velocity (U_m) was 5600. In the plane-impinging-jet case, the Reynolds number based on the nozzle width (D) and the center velocity at the nozzle exit (U_0) was 6000. Concerning the obstacle-flow case, the Reynolds number based on the

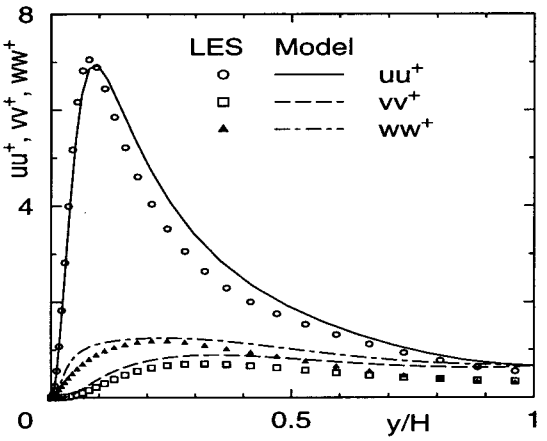

Figure 3: Comparison of Reynolds normal stresses in channel flow ($Re = 2U_m H/\nu = 5600$).

obstacle height (H) and the mean velocity on the obstacle (U_H) was 3350. In this study, the Prandtl number (P_r) was set to 0.71 for all the cases. The schematic views of the plane-impinging-jet and obstacle-flow cases are illustrated in Figs. 1 and 2, respectively. The present computational conditions are summarized in Table 1.

All the calculations were performed with the finite-volume procedure STREAM of Lien and Leschziner (1994), followed by several improvements and substantially upgraded by Apsley and Leschziner (2000). In this study, a priori tests were performed for all the cases by using the LES data for velocity fields. Furthermore, to investigate their applicability in more detail, calculations with an algebraic velocity-field model were conducted for the first two cases. In calculating flow fields, we adopted a recently-developed model by Abe et al. (2003) (AJL model), which was based on the previously-proposed model by Abe et al. (1997) followed by some effective modifications for predicting Reynolds-stress anisotropy more correctly. Summary of the AJL model is presented in Appendix A.

RESULTS AND DISCUSSION

Plane Channel Flow

Figure 3 compares the Reynolds normal stresses predicted by the AJL model with those of the LES data (Abe and Suga, 2001a), where $\overline{uu}$, $\overline{vv}$ and $\overline{ww}$ are, respectively, the streamwise, the wall-normal and the spanwise components of the Reynolds-stress tensor. The obtained results are in good agreement with the LES data, including the wall-limiting behavior of the wall-normal component.

Predictive performance of the scalar fluxes by the GGDH and the quadratic models are compared in Fig. 4, where a priori test was performed for the scalar field with the aid of the LES data for the velocity field. Note that the dissipation rate was obtained from the residual of the turbulence-energy budget. On the other hand, Fig. 5 illustrates the results in case that the AJL model was used for the velocity-field calculation. As for the channel-flow case, both results in Figs. 4 and 5 show a similar trend that the quadratic model provides reasonable prediction for both $\overline{ut}$ and $\overline{vt}$, while the GGDH model fails to do it. In this case, the above results seem natural because the AJL model provides reasonable predictions not only for the mean velocity but also for the

Table 1: Computational conditions.

	Domain	Grid	Re	Pr	B. C.
Channel flow	2H	54	$Re = 5600$	0.71	no-slip wall, $T_{lower} = 0$, $T_{upper} = 1$
Plane impinging jet	20D × 10D	115 × 87	$Re = 6000$	0.71	no-slip wall, $T_{in} = 0$, $T_{wall} = 1$
Obstacle flow	31H × 2H	243 × 71	$Re = 3350$	0.71	no-slip wall, $T_{lower} = 0$, $T_{upper} = 1$

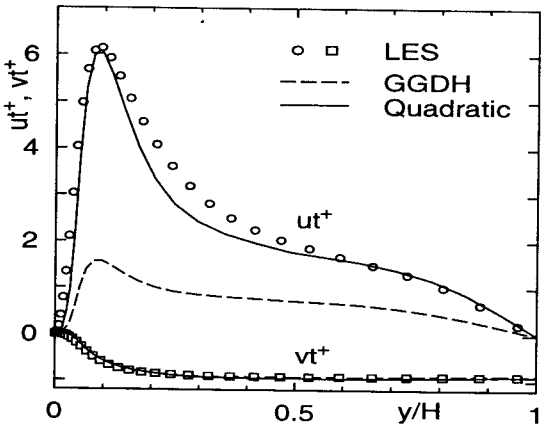

Figure 4: Comparison of turbulent scalar fluxes by using LES data for velocity field (a priori tests, $P_r = 0.71$).

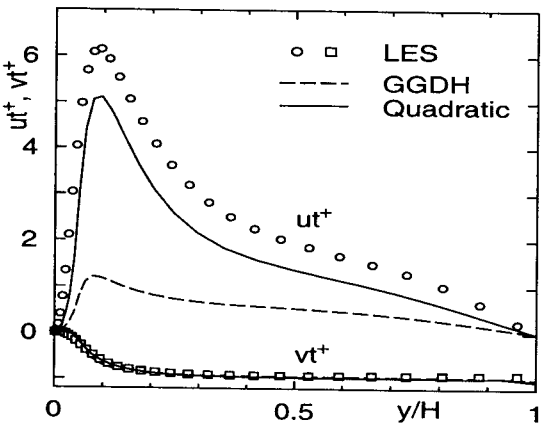

Figure 5: Comparison of turbulent scalar fluxes by using AJL model for velocity-field calculation ($P_r = 0.71$).

stress anisotropy in the near-wall region. This fact also coincides well with the knowledge obtained from Abe and Suga (2001a).

Plane Impinging Jet

Figures 6 – 9 show representative results for the plane-impinging-jet case. Figure 6 compares the Reynolds normal stresses in the wall-jet region ($x/D = 4$) with the LES data (Abe and Suga, 2001b). It is seen that generally good agreement is obtained. In particular, the wall-normal component ($\overline{vv}$) is predicted very well in the near-wall region. The predicted scalar-fluxes in the near-wall region were compared in Fig. 7. The results from both a priori tests and calculations with the AJL model show that the quadratic model returns much more reasonable $\overline{ut}$ than the GGDH model does. As for the GGDH model, the level of C_{t1} seems reasonable to predict $\overline{vt}$, while $\overline{ut}$ can never be predicted precisely with the same model constant.

The predicted Reynolds normal stresses in the stagnation region were shown in Fig. 8. Although the prediction accuracy of the AJL model is not adequate especially for the separation between $\overline{uu}$ and $\overline{ww}$, the wall-normal turbulence ($\overline{vv}$) is predicted well even in the stagnation region. This is important to predict $\overline{vt}$ by the GGDH model. Figure 9 compares the predicted scalar fluxes with the LES data. As for the results of a priori test, $\overline{vt}$ is a little overestimated by the GGDH model and considerably underestimated by the quadratic model. On the other hand, the results with the AJL model indicate that the GGDH model returns good agreement with the LES data, although a little underprediction is seen. The quadratic model returns considerable underestimation of $\overline{vt}$. Interesting is that even in the stagnation region, C_{t1} at a similar level to that in the channel-flow case may be applicable to the prediction of scalar fluxes, while the quadratic model may have some difficulty for applications of this kind.

Obstacle Flow

Figure 10 illustrates the Reynolds normal stresses obtained from the LES data (Abe and Suga, 2001b). In the figure, the location at $x/H = 7$ is just around the reattachment point, while $x/H = -6$ is actually in the redeveloping region between obstacles due to the periodic condition in the x-direction. From Fig. 10 (a), it is seen that stress anisotropy shows a similar trend to that in the channel-flow case. On the other hand, Fig. 10 (b) shows a considerable different aspect in the region close to the lower wall, where the separation between $\overline{uu}$ and $\overline{ww}$ becomes very small, while in the upper-wall region, $\overline{uu}$ is still much larger than $\overline{ww}$. The turbulent state in the lower-wall region is characterized by that encountered in axisymmetric contraction.

The scalar-fluxes obtained from a priori test were compared in Fig. 11. From Fig. 11 (a), the results show a similar trend to that in the channel-flow case. The quadratic model successfully predicts the streamwise scalar flux as well as the wall-normal one, while the GGDH model fails to do it. Also is shown from Fig. 11 (b) that in the upper-wall region at $x/H = 7$, the quadratic model generally provides good prediction of the scalar-flux vector, though a little underprediction is seen. This fact reasonably coincides with the characteristics of the Reynolds-stress anisotropy shown in Fig. 10 (b). On the contrary, it is understood from Fig. 11 (b) that in the region very close to the lower-wall, i.e., $y/H < 0.1$, the streamwise scalar flux by the LES is situated between those predicted by the GGDH and the quadratic models, while the quadratic model works well a little away

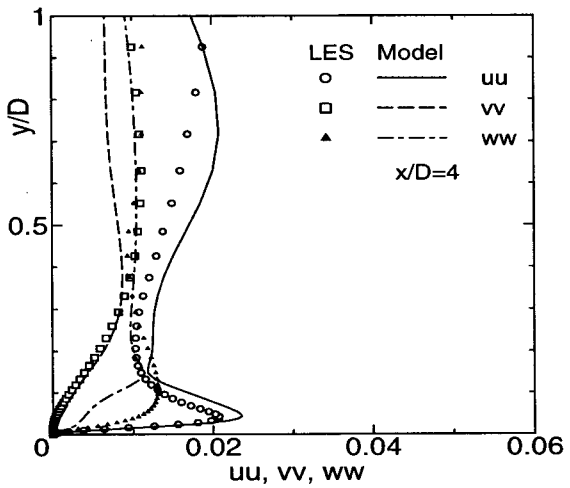

Figure 6: Comparison of Reynolds normal stresses in wall-jet region of plane impinging jet.

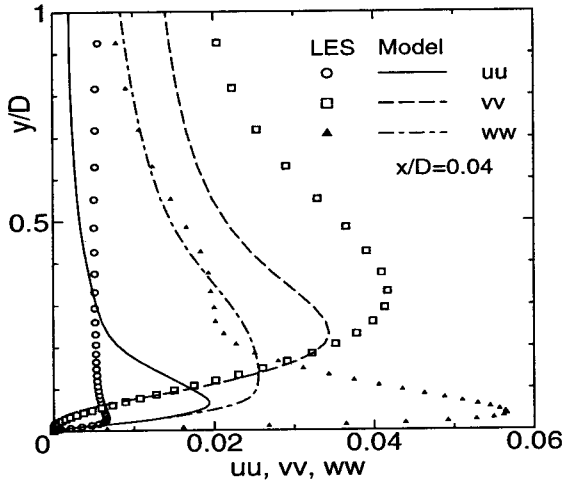

Figure 8: Comparison of Reynolds normal stresses in stagnation region of plane impinging jet.

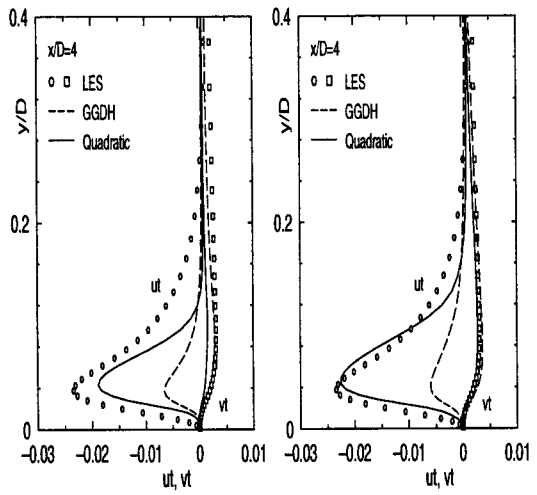

(a) a priori (b) AJL model

Figure 7: Comparison of turbulent scalar fluxes in wall-jet region of plane impinging jet ($P_r = 0.71$).

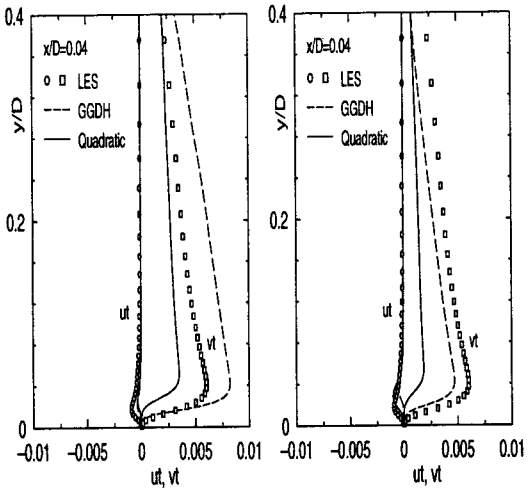

(a) a priori (b) AJL model

Figure 9: Comparison of turbulent scalar fluxes in stagnation region of plane impinging jet ($P_r = 0.71$).

from the wall surface, i.e., $y/H > 0.1$. Also is shown that both models successfully predict the wall-normal scalar flux with the same model constant as in the channel-flow case even in the region around the reattachment point.

Among algebraic scalar-flux models previously proposed, the SA model (Suga and Abe, 2000) is one of representatives to take account of the above characteristics in complex scalar-transfer fields. The SA model has a combined formulation of the GGDH and the quadratic forms based on Eq. (3). In this model, the model constants were calibrated as $C_{t1} \sim 0.06$ and $C_{t2} \sim 0.4$ with highly-functionalized low-Reynolds-number model functions. Such small value of C_{t1} gives a strong influence to reduce scalar fluxes in regions where the GGDH part plays a dominant role. On the other hand, it has been pointed out from previous studies that higher turbulent Prandtl number or similar effect needs to be incorporated into eddy-viscosity-type models for reasonable scalar-transfer predictions in the reattachment region (Abe et al., 1995). This treatment also has the capability of reducing an excessive turbulent length scale for the scalar-field prediction.

Considering the facts obtained from the present results, however, it is indicated that model constants at the same level as in the channel-flow case may be used for predicting scalar fluxes even in complex turbulence with impingement and separation. For example, as for the SA model, the level of C_{t2} (~ 0.4) is confirmed to be reasonable in the wall-shear region, including a wall-jet region of plane impinging jet and a redeveloping region of obstacle flow. Concerning C_{t1}, however, its value (~ 0.06) may be too small to predict scalar-transfer coefficient correctly if the GGDH part is modeled to be indeed dominant especially in the stagnation

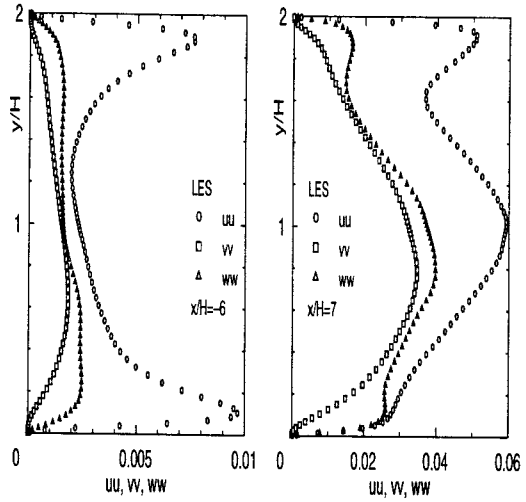

(a) $x/H = -6$ (b) $x/H = 7$

Figure 10: Reynolds normal stresses in obstacle flow (LES data).

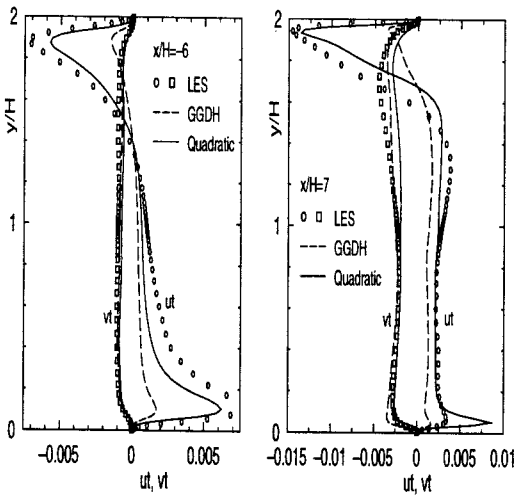

(a) $x/H = -6$ (b) $x/H = 7$

Figure 11: Comparison of turbulent scalar fluxes in obstacle flow ($P_r = 0.71$, a priori test).

region of a plane impinging jet. To discuss on this topic in more detail, further investigation of the performance of the SA model is thought to be useful.

CONCLUDING REMARKS

To reveal unknown characteristics of algebraic turbulent scalar-flux models, detailed investigations of some representative model expressions for scalar fluxes were performed in several complex turbulent flows with impingement and separation. The main conclusions derived from the study are as follows:

- As regards the angle of scalar-flux vector, it has been confirmed again that the modeling concept proposed by Abe and Suga (2001a, 2001b) is basically applicable to complex flow fields with impingement and separation.
- In this sense, a combined model of the GGDH and the quadratic forms proposed by Suga and Abe (2000), i.e., the SA model, is thought to be a reasonable approach to predict such complex scalar-transfer fields.
- In this study, however, the results indicate that the GGDH part of the SA model (i.e., $C_{t1} \sim 0.06$) may be too small to predict scalar-transfer coefficient correctly in stagnation and reattachment regions if the GGDH part indeed plays a dominant role there.
- To construct a higher-performance algebraic scalar-flux model, further discussion on the constants and functions bridging the GGDH and the quadratic forms is needed. As a good example, detailed investigation of the performance of the SA model is expected to be useful for further development.

ACKNOWLEDGEMENTS

The author wishes to express his appreciation to Professor M.A. Leschziner of Imperial College for the support in using the STREAM code.

APPENDIX A. SUMMARY OF TURBULENCE MODEL

The following is the summary of the AJL model (Abe et al., 2003) used in the present study, which is categorized in the two-equation nonlinear eddy-viscosity model. In what follows, use is made of the anisotropy tensor b_{ij}, the strain-rate tensor S_{ij} and the vorticity tensor Ω_{ij}:

$$b_{ij} = \frac{\overline{u_i u_j}}{2k} - \frac{\delta_{ij}}{3}, \quad S_{ij} = \frac{\overline{U}_{i,j} + \overline{U}_{j,i}}{2}, \quad \Omega_{ij} = \frac{\overline{U}_{i,j} - \overline{U}_{j,i}}{2} \tag{5}$$

These are normalized with a model constant and a turbulent time scale as

$$b^*_{ij} = C_D\, b_{ij}, \quad S^*_{ij} = C_D \tau S_{ij}, \quad \Omega^*_{ij} = C_D \tau \Omega_{ij} \tag{6}$$

where

$$\tau = \frac{\nu_t}{k}, \quad \nu_t = C_\mu f_\mu \frac{k^2}{\varepsilon}, \quad C_D = 0.8, \quad C_\mu = 0.12 \tag{7}$$

To represent the damping effects of viscosity, use is made of Abe et al's (1997) damping function:

$$f_\mu = \left[1 + \frac{35}{R_t^{\frac{3}{4}}} \exp\left\{-\left(\frac{R_t}{30}\right)^{\frac{3}{4}}\right\}\right] \{1 - f_w(26)\} \tag{8}$$

where

$$f_w(\xi) = \exp\left\{-\left(\frac{n^*}{\xi}\right)^2\right\} \tag{9}$$

In Eqs. (8) and (9), $R_t (= k^2/\nu\varepsilon)$ is the turbulent Reynolds number, $n^* (= (\nu\varepsilon)^{1/4} n/\nu)$ is the non-dimensional wall distance with Kolmogorov scale (Abe et al., 1994) and ξ is a prescribed constant. The Reynolds stresses may be evaluated from Eqs. (5) and (6) as follows:

$$\overline{u_i u_j} = \frac{2}{3} k \delta_{ij} + 2k\, b_{ij} = \frac{2}{3} k \delta_{ij} + 2k \left(\frac{b^*_{ij}}{C_D}\right) \tag{10}$$

The general form of the constitutive equation for the anisotropy tensor b^*_{ij} is:

$$b^*_{ij} = {}^1b^*_{ij} + \{1 - f_w(26)\} \left\{{}^2b^*_{ij} + {}^sb^*_{ij}\right\} + {}^wb^*_{ij} \tag{11}$$

The basic constitutive relations for ${}^1b^*_{ij}$ and ${}^2b^*_{ij}$ are those proposed by Abe et al. (1997).

$$ {}^1b^*_{ij} = -C_B S^*_{ij} \,, $$

$$ {}^2b^*_{ij} = C_B \left\{ -2\left(S^*_{ik}\Omega^*_{kj} - \Omega^*_{ik}S^*_{kj}\right) + 2\left(S^*_{ik}S^*_{kj} - \frac{\delta_{ij}}{3}S^{*2}\right) \right\} \tag{12} $$

In Eq. (12), the coefficient C_B is as follows:

$$ C_B = \frac{1}{1 + \frac{22}{3}\Omega^{*2} + \frac{2}{3}\left(\Omega^{*2} - S^{*2}\right) f_B} \tag{13} $$

where

$$ f_B = 1 + C_\eta \left(\Omega^* - S^*\right), \quad S^{*2} = S^*_{mn}S^*_{mn}, \quad \Omega^{*2} = \Omega^*_{mn}\Omega^*_{mn}, $$

$$ S^* = \sqrt{S^{*2}}, \quad \Omega^* = \sqrt{\Omega^{*2}}, \quad C_\eta = 100 \tag{14} $$

In addition to the above, the following two fragments are introduced. The first fragment is incorporated for strong straining field:

$$ {}^s b^*_{ij} = -C_B f_{s1} S^*_{ij} + 2C_B f_{s2}\left(S^*_{ik}S^*_{kj} - \frac{\delta_{ij}}{3}S^{*2}\right) \tag{15} $$

where

$$ f_{s1} = f_{r1} f_{r2} C_{s1}\left(\Omega^{*2} - S^{*2}\right), $$

$$ f_{s2} = -f_{r1} f_{r2}\left\{1 + C_{s2}\left(\Omega^* - S^*\right)\right\}, $$

$$ f_{r1} = \frac{\Omega^2 - S^2}{\Omega^2 + S^2}, \quad f_{r2} = \frac{S^2}{\Omega^2 + S^2}, \quad S^2 = S_{mn}S_{mn}, $$

$$ \Omega^2 = \Omega_{mn}\Omega_{mn}, \quad C_{s1} = 0.15C_\eta, \quad C_{s2} = 0.07C_\eta \tag{16} $$

The second fragment is introduced to improve the predictive performance in the near-wall region:

$$ {}^w b^*_{ij} = C_D \; f_w(26) \; {}^w b_{ij} \tag{17} $$

where

$$ {}^w b_{ij} = -\alpha_w \frac{1}{2}\left(d_i d_j - \frac{\delta_{ij}}{3} d_k d_k\right) $$

$$ + \left(1 - {f_{r1}}^2\right)\left\{ -\frac{\beta_w C_w}{1 + C_w\sqrt{S^{**2}\Omega^{**2}}}\left(S^{**}_{ik}\Omega^{**}_{kj} - \Omega^{**}_{ik}S^{**}_{kj}\right) \right. $$

$$ \left. + \frac{\gamma_w C_w}{1 + C_w S^{**2}}\left(S^{**}_{ik}S^{**}_{kj} - \frac{\delta_{ij}}{3}S^{**2}\right)\right\} \tag{18} $$

In Eq. (18),

$$ S^{**}_{ij} = \tau_d S_{ij}, \quad \Omega^{**}_{ij} = \tau_d \Omega_{ij}, $$

$$ S^{**2} = S^{**}_{mn}S^{**}_{mn}, \quad \Omega^{**2} = \Omega^{**}_{mn}\Omega^{**}_{mn}, $$

$$ \alpha_w = 1, \quad \beta_w = \frac{1}{4}, \quad \gamma_w = 1.5, \quad C_w = 0.5, $$

$$ d_i = \frac{N_i}{\sqrt{N_k N_k}}, \quad N_i = \frac{\partial l_d}{\partial x_i}, \quad l_d = n \tag{19} $$

where n is the nearest wall distance and the time scale τ_d is modeled as follows:

$$ \tau_d = \left\{1 - f_w(15)\right\}\frac{k}{\varepsilon} + f_w(15)\sqrt{\frac{\nu}{\varepsilon}} \tag{20} $$

Turbulence energy is determined from the usual form of the transport equation:

$$ \frac{\mathrm{D}k}{\mathrm{D}t} = \frac{\partial}{\partial x_j}\left\{\left(\nu + \frac{\nu_t}{\sigma_k}\right)\frac{\partial k}{\partial x_j}\right\} - \overline{u_i u_j}\frac{\partial \overline{U}_i}{\partial x_j} - \varepsilon \tag{21} $$

where

$$ \sigma_k = \frac{1.2}{f_t}, \quad f_t = 1 + 5.0 f_w(5) \tag{22} $$

The dissipation-rate equation is that proposed by Abe et al. (1997) with minor modifications:

$$ \frac{\mathrm{D}\varepsilon}{\mathrm{D}t} = \frac{\partial}{\partial x_j}\left\{\left(\nu + \frac{\nu_t}{\sigma_\varepsilon}\right)\frac{\partial \varepsilon}{\partial x_j}\right\} - C_{\varepsilon 1}\frac{\varepsilon}{k}\overline{u_i u_j}\frac{\partial \overline{U}_i}{\partial x_j} - C_{\varepsilon 2} f_\varepsilon \frac{\varepsilon^2}{k} \tag{23} $$

where

$$ f_\varepsilon = \left[1 - 0.3\exp\left\{-\left(\frac{R_t}{6.5}\right)^2\right\}\right]\left\{1 - f_w(3.3)\right\}, $$

$$ C_{\varepsilon 1} = 1.45, \quad C_{\varepsilon 2} = 1.83, \quad \sigma_\varepsilon = \frac{1.5}{f_t} \tag{24} $$

REFERENCES

Abe, K., Kondoh, T. and Nagano, Y., 1994, "A New Turbulence Model for Predicting Fluid Flow and Heat Transfer in Separating and Reattaching Flows - I. Flow Field Calculations," *Int. J. Heat Mass Transfer*, Vol. 37, pp. 139-151.

Abe, K., Kondoh, T. and Nagano, Y., 1995, "A New Turbulence Model for Predicting Fluid Flow and Heat Transfer in Separating and Reattaching Flows - II. Thermal Field Calculations," *Int. J. Heat Mass Transfer*, Vol. 38, pp. 1467-1481.

Abe, K., Kondoh, T. and Nagano, Y., 1997, "On Reynolds-Stress Expressions and Near-Wall Scaling Parameters for Predicting Wall and Homogeneous Turbulent Shear Flows," *Int. J. Heat Fluid Flow*, Vol. 18, pp. 266-282.

Abe, K. and Suga, K., 2001a, "Towards the Development of a Reynolds-Averaged Algebraic Turbulent Scalar-Flux Model," *Int. J. Heat Fluid Flow*, Vol. 22, pp. 19-29.

Abe, K. and Suga, K., 2001b, "Large Eddy Simulation of Passive Scalar in Complex Turbulence with Flow Impingement and Flow Separation," *Heat Transfer Asian Research*, Vol. 30, pp. 402-418.

Abe, K., Jang, Y.J. and Leschziner, M.A., 2003, "An Investigation of Wall-Anisotropy Expressions and Length-Scale Equations for Non-Linear Eddy-Viscosity Models," *Int. J. Heat Fluid Flow*, Vol. 24, pp. 181-198.

Apsley, D.D. and Leschziner, M.A., 2000, "Advanced Turbulence Modelling of Separated Flow in a Diffuser," *Flow, Turbulence and Combustion*, Vol. 63, pp. 81-112.

Daly, B.J. and Harlow, F.H., 1970, "Transport equations in turbulence," *Phys. Fluids*, Vol. 13, pp. 2634-2649.

Durbin P.A., 1993, "Application of a Near-Wall Turbulence Model to Boundary Layers and Heat Transfer," *Int. J. Heat Fluid Flow*, Vol. 14, pp. 316-323.

Kim, J. and Moin, P, 1989, "Transport of Passive Scalars in a Turbulent Channel Flows," *Turbulent Shear Flows 6*, pp. 85-96 (Springer).

Lien, F.S. and Leschziner, M.A., 1994, "Upstream Monotonic Interpolation for Scalar Transport with Application to Complex Turbulent Flows," *Int. J. Num. Meths. in Fluids*, Vol. 19, pp. 527-548.

Launder, B.E., 1976, *Turbulence (Edited by Bradshaw, P.)*, pp. 231-287 (Springer).

Suga, K. and Abe, K., 2000, "Nonlinear Eddy Viscosity Modelling for Turbulence and Heat Transfer Near Wall and Shear Free Boundaries," *Int. J. Heat Fluid Flow*, Vol. 21, pp. 37-48.